





Aggregating Multidimensional Wireless Link Information for Device-Free Localization

Dongping Yu , Yan Guo , Ning Li, and Sixing Yang

College of Communications Engineering, Army Engineering University of PLA,
Nanjing 210007, China
guoyan.1029@sina.com

Abstract. Device-free localization (DFL) is an emerging and promising technique, which can realize target localization without the requirement of attaching any wireless devices to targets. By analyzing the shadowing loss caused by targets on wireless links, we can estimate the target locations. However, for existing DFL approaches, a large number of wireless links is required to guarantee a certain localization precision, which may lead to high hardware cost. In this paper, we propose a novel multi-target device-free localization method with multidimensional wireless link information (MDMI). Unlike previous works that measure RSS only on a single transmission power level, MDMI collects RSS measurements from multiple transmission power levels to enrich the measurement information. Furthermore, the compressive sensing (CS) theory is applied by exploiting the inherent spatial sparsity of DFL. We model the DFL problem as a joint sparse recovery problem and adopt the multiple sparse Bayesian learning (M-SBL) algorithm to reconstruct the sparse vectors of different transmission power levels. Numerical simulation results demonstrate the outstanding performance of the proposed method.

Keywords: Device-free localization · Wireless sensor network · Compressive sensing · Sparse Bayesian learning

1 Introduction

In the last decade, target localization has grasped great attention since it is pivotal in many location-based services (LBS). To address the localization problem of multiple targets, an intense research work has been carried out by the scientific community [1]. With the widespread usage of wireless networks, target location estimation can be realized by analyzing the target-induced perturbations in the radio frequency (RF) field. Based on this insight, the device-free localization (DFL) [2,3] has been proposed, which do not require targets to carry any wireless devices, nor to participate actively in the localization process. It is attractive

and promising for a wide number of applications, such as intrusion detection, emergency rescue, healthcare, and smart spaces, etc. [4].

The DFL technique can enable existing wireless infrastructures (e.g., WiFi, WSNs, Bluetooth, etc.) to have the ability of location awareness while, at the same time, do not disturb the normal communication tasks. Received signal strength (RSS) is a common signature of target location. In the literature, many RSS-based multi-target DFL approaches have been developed. Based on how to utilize the RSS measurements, there are three types of DFL approaches, including geometry-based approaches, fingerprinting-based approaches, and radio tomographic imaging (RTI)-based approaches. The geometry-based approaches exploit the geometry information of shadowed links to locate targets [5]. However, they need a prior knowledge of the deployment of wireless nodes, and suffer from low localization accuracy. The fingerprinting-based DFL approaches can achieve an improved accuracy [6], whereas a labor-intensive and time-consuming training process is required to build and update the radio map. The RTI-based approaches [7] infer the target positions according to the principle of computed tomography (CT). They use an empirical model to quantify the relationship between RSS variations and target locations. Unfortunately, a sufficient number of wireless links is required to cover the area of interest.

As a new and promising technique, the compressive sensing (CS) [8] theory asserts that a small number of measurements (undersampled) will suffice for recovering signals that are compressible or sparse under a certain basis. Recent works have shown the potential of applying the CS theory in multi-target DFL. Compared to traditional DFL approaches, the CS-based DFL method demands much less number of wireless links (or measurements). As a representative CS-based DFL method, LCS [9] has proven that the product of the dictionary obeys restricted isometry property (RIP) with high probability. Different with LCS, E-HIPA [10] does not require a prior knowledge of target number. It adopts an adaptive orthogonal matching pursuit algorithm to reconstruct the sparse location vector. Moreover, in order to adapt to the changes in radio environments, DR-DFL [11] presents a dictionary refinement algorithm.

However, existing CS-based multi-target DFL approaches collect RSS measurements from just one transmission power level. It is assumed that each wireless link can only provide one reading of the RSS. To enrich the measurement information, MDMI proposes to collect RSS measurements from multiple transmission power levels. By doing so, the performance of multi-target DFL can be further improved with the assistance of power diversity. Hence, better localization accuracy can be achieved without increasing the number of wireless links. To leverage the advantage of CS in sparse recovery, we model the multi-target DFL with multiple transmission power levels as a joint sparse recovery problem. The sparse vectors corresponding to different transmission power levels share a common sparsity pattern. We reconstruct them by using the multiple sparse Bayesian learning (M-SBL) algorithm [12], and estimate the number and locations of multiple targets according to the reconstructed sparse vectors. The rest of the paper is organized as follows: In Sect. 2, we give the signal model

and model the DFL problem as a joint sparse recovery problem. The design and implementation of the proposed MDMI method are illustrated in Sect. 3, and the simulation results are shown in Sect. 4. Finally, conclusions are given in Sect. 5.

2 Problem Statement and Motivation

2.1 Problem Statement

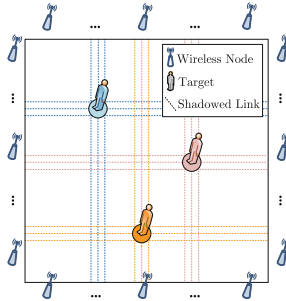


Fig. 1. Illustration of multi-target device-free localization.

Suppose a wireless network is deployed in the area of interest. When multiple targets entering into the area, some wireless links will be shadowed. As a consequence, the RSS readings on these shadowed links may be different from the measurements when no target is present. Our MDMI method attempt to leverage the changes of RSS to realize target localization. For simplicity, an illustration of the CS-based multi-target DFL is shown in Fig. 1. The wireless nodes are uniformly deployed around the perimeter of the monitoring area \mathcal{A} , and K targets are randomly distributed in it. We divide \mathcal{A} into N equal-sized grids, thus the target locations can be represented as

$$\boldsymbol{\theta} = [\theta_1, \theta_2, \dots, \theta_n, \dots, \theta_N]^T \quad (1)$$

where $\boldsymbol{\theta} \in \mathbb{R}^{N \times 1}$ denotes the location vector, $\theta_n \in \{0, 1\}$ denotes the n -th entry of $\boldsymbol{\theta}$. If there is a target in grid n , we set $\theta_n = 1$; otherwise $\theta_n = 0$. In this sense, K also represents the sparsity level of $\boldsymbol{\theta}$. The aim of the CS-based DFL is equivalent to reconstruct $\boldsymbol{\theta}$ by exploiting RSS measurements.

According to the shadowing model, the RSS measurement of link m with transmission power level e can be given as

$$R(m, e) = G(m, e) + P(m, e) - L(m, e) - 10\beta \lg d_m - S(m, e) + \epsilon(m, e) \quad (2)$$

where $G(m, e)$ denotes the receiver gain (dB), $P(m, e)$ is the transmission power, $L(m, e)$ is the signal attenuation power of unit distance, β is the path-loss exponent, and d_m represents the length of link m . The above-mentioned parameters

are constant with time. On the contrary, $S(m, e)$ and $\epsilon(m, e)$ are time-variant parameters. $S(m, e)$ denotes the shadowing loss, which is caused by the targets that attenuate radio signals. $\epsilon(m, e)$ is the measurement noise. We denote $R_0(m, e)$ as the RSS measurement when \mathcal{A} is vacant. Then, the change of RSS corresponding to link m and transmission power level e can be written as

$$\Delta R(m, e) = R(m, e) - R_0(m, e) \approx -S(m, e) + \epsilon(m, e) - \epsilon_0(m, e) \quad (3)$$

As mentioned earlier, \mathcal{A} is divided into multiple grids. Hence, we approximate $S(m, e)$ by the summation of attenuation that occurs in each grid, i.e.,

$$\Delta R(m, e) = \sum_{n=1}^N \Delta p_n(m, e) \cdot \theta_n + \Delta \epsilon(m, e) \quad (4)$$

where $\Delta p_n(m, e)$ denotes the shadowing loss on link m that contributed by a target in grid n . $\Delta \epsilon(m, e)$ is the change of measurement noise. Based on the saddle surface (SaS) model [13], $\Delta p_n(m, e)$ can be calculated as

$$\Delta p_n(m, e) = \left(\frac{1 - \rho}{\lambda_1^2} U_{m,n}^2 + \rho \cdot \left(1 - \frac{V_{m,n}^2}{\lambda_2^2} \right) \right) \cdot \gamma^e \quad (5)$$

where $(U_{m,n}, V_{m,n})$ is the coordinate of grid n . According to the SaS model, only the grids in the elliptical spatial impact area of link m will have a nonzero $\Delta p_n(m, e)$, and $\Delta p_n(m, e)$ is very different at different locations within the spatial impact area. In this model, ρ represents the shadow rate, which is defined as the normalized shadowing effect in the midpoint of the line-of-sight (LOS) path. γ^e denotes the maximum shadowing effect corresponding to power level e . Based on (4), the RSS variations on M links can be expressed as

$$\mathbf{y}^e = \Phi^e \boldsymbol{\theta} + \boldsymbol{\epsilon}^e \quad (6)$$

where $\mathbf{y}^e \in \mathbb{R}^{M \times 1}$ is the measurement vector corresponding to power level e , $\Phi^e \in \mathbb{R}^{M \times N}$ is a dictionary, and $\boldsymbol{\epsilon}^e \in \mathbb{R}^{M \times 1}$ is the noise vector. We denote $\phi_{m,n}^e$ as the (m, n) -th element of Φ^e , which is equal to $\Delta p_n(m, e)$.

2.2 Motivation

In fact, $\Delta p_n(m, e)$ can be decomposed as $\Delta p_n(m, e) = (\phi_{m,n}^e / \gamma^e) \cdot \gamma^e$. We define $\mathbf{w}^e = \gamma^e \cdot \boldsymbol{\theta}$ and $\phi_{m,n} = (\phi_{m,n}^e / \gamma^e)$. It is assumed that we can collect RSS measurements from E different transmission power levels. Thus, the CS-based DFL can be reformulated as a joint sparse recovery problem as follows:

$$\mathbf{Y} = \Phi \mathbf{W} + \Xi \quad (7)$$

where $\mathbf{Y} \in \mathbb{R}^{M \times E}$ is the measurement matrix, and $\mathbf{Y} = [\mathbf{y}^1, \dots, \mathbf{y}^E]$. $\Xi \in \mathbb{R}^{M \times E}$ is the noise matrix, and $\Xi = [\boldsymbol{\epsilon}^1, \dots, \boldsymbol{\epsilon}^E]$. $\Phi \in \mathbb{R}^{M \times N}$ is a dictionary, whose

(m, n) -th element is $\phi_{m,n}$. $\mathbf{W} \in \mathbb{R}^{N \times E}$ is a coefficient matrix, whose e -th component \mathbf{w}^e is a K -sparse coefficient vector. \mathbf{W} satisfies $rd(\mathbf{W}) = K$, where

$$rd(\mathbf{W}) \triangleq \sum_{n=1}^N \mathcal{I}[\|W_n\| > 0] \quad (8)$$

$rd(\cdot)$ represents a row-diversity measure, which counts the number of rows that have nonzero values. $\mathcal{I}[\cdot]$ denotes the indicator function. $\|\cdot\|$ is an arbitrary vector norm, and W_n is the n -th row of \mathbf{W} . To reconstruct \mathbf{W} , we formulate the following relaxed optimization problem:

$$\hat{\mathbf{W}} = \arg \min_{\mathbf{W}} (\|\mathbf{Y} - \Phi \mathbf{W}\|_{\mathcal{F}}^2 + \ell \cdot rd(\mathbf{W})) \quad (9)$$

where $\|\cdot\|_{\mathcal{F}}$ denotes the Frobenius norm, ℓ is a tradeoff parameter, and $rd(\mathbf{W})$ is the regularization term. However, directly solving (9) is NP-hard, and the optimal value of ℓ is generally not available.

3 Joint Sparse Recovery

To bypass the requirement of estimating ℓ , we resort to a Bayesian probabilistic approach. By applying an $\exp[-(\cdot)]$ transformation, the optimization problem in (9) can be viewed as a maximum a posterior probability (MAP) estimation task, which is summarized as follows:

$$\hat{\mathbf{W}} = \arg \max_{\mathbf{W}} p(\mathbf{Y} | \mathbf{W}) \cdot p(\mathbf{W}) = \arg \max_{\mathbf{W}} p(\mathbf{W} | \mathbf{Y}) \quad (10)$$

To solve the above problem, we resort to the M-SBL algorithm. Firstly, a Gaussian distribution is imposed on the likelihood function for each \mathbf{y}^e and \mathbf{w}^e , i.e.,

$$p(\mathbf{y}^e | \mathbf{w}^e, \sigma) = (2\pi\sigma^2)^{-\frac{N}{2}} \exp\left(-\frac{\|\mathbf{y}^e - \Phi \mathbf{w}^e\|_2^2}{2\sigma^2}\right) \quad (11)$$

where σ^2 denotes the noise variance. Secondly, to induce the sparsity of \mathbf{w}^e , a Gaussian prior is imposed on the n -th row of \mathbf{W} , i.e.,

$$p(W_n; \alpha_n) = \mathcal{N}(0, \alpha_n \mathbf{I}) \quad (12)$$

where α_n denotes the common variance of the elements in W_n . Here, $\{\alpha_1, \dots, \alpha_N\}$ is used for encouraging the joint sparsity of $\{\mathbf{w}^1, \dots, \mathbf{w}^E\}$. Based on (12), the prior distribution of \mathbf{W} can be given as

$$p(\mathbf{W}; \boldsymbol{\alpha}) = \prod_{n=1}^N p(W_n; \alpha_n) \quad (13)$$

where $\boldsymbol{\alpha} = [\alpha_1, \dots, \alpha_N]^T$. Based on the likelihood function and the prior distributions, the posterior of \mathbf{w}^e can be written as

$$p(\mathbf{w}^e | \mathbf{y}^e; \alpha_n) = \frac{p(\mathbf{w}^e, \mathbf{y}^e; \boldsymbol{\alpha})}{\int p(\mathbf{w}^e, \mathbf{y}^e; \boldsymbol{\alpha}) d\mathbf{w}^e} = \mathcal{N}(\boldsymbol{\mu}_e, \boldsymbol{\Sigma}) \quad (14)$$

where Σ denotes the covariance matrix. It can be given as

$$\Sigma = \text{Cov}[\mathbf{w}^e | \mathbf{y}^e; \boldsymbol{\alpha}] = \mathbf{\Gamma} - \mathbf{\Gamma} \mathbf{\Phi}^T \mathbf{\Theta}^{-1} \mathbf{\Phi} \mathbf{\Gamma} \quad (15)$$

where $\mathbf{\Gamma} = \text{diag}(\boldsymbol{\alpha})$ and $\mathbf{\Theta} = \sigma^2 \mathbf{I} + \mathbf{\Phi} \mathbf{\Gamma} \mathbf{\Phi}^T$. The mean of \mathbf{W} is

$$\mathbf{\Pi} = [\boldsymbol{\mu}_1, \dots, \boldsymbol{\mu}_E] = \text{E}[\mathbf{W} | \mathbf{Y}; \boldsymbol{\alpha}] = \mathbf{\Gamma} \mathbf{\Phi}^T \mathbf{\Theta}^{-1} \mathbf{Y} \quad (16)$$

The e -th column of $\mathbf{\Pi}$ represents the mean vector of \mathbf{w}^e . To find the optimal value of $\boldsymbol{\alpha}$, we maximize the marginal likelihood with respect to $\boldsymbol{\alpha}$. Based on it, the cost function can be expressed as

$$\mathcal{L}(\boldsymbol{\alpha}) = -2 \log \int p(\mathbf{Y}, \mathbf{W}) p(\mathbf{W}) d\mathbf{W} = E \cdot \log |\mathbf{\Theta}| + \sum_{e=1}^E (\mathbf{y}^e)^T \mathbf{\Theta}^{-1} \mathbf{y}^e \quad (17)$$

From (17), the update rule of α_n can be given as

$$\alpha_n^* = \frac{1}{E} \|\Pi_{n \cdot}\|_2^2 + \Sigma_{nn}, \quad \forall n = 1, \dots, N \quad (18)$$

In the same way, σ^2 can be updated as

$$(\sigma^2)^* = \frac{\frac{1}{E} \|\mathbf{Y} - \mathbf{\Phi} \mathbf{\Pi}\|_{\mathcal{F}}^2}{M - N + \sum_{n=1}^N \frac{\Sigma_{nn}}{\alpha_n}} \quad (19)$$

We estimate the posterior of \mathbf{W} and the parameters $\boldsymbol{\alpha}$ and σ^2 by maximizing a marginal likelihood function via an iterative algorithm, which is summarized in Algorithm 1. To estimate target locations, a sparse vector $\Pi_{\cdot \hat{e}}$ is chosen from $\mathbf{\Pi}$. In step 10, a sparsity threshold η_{th} is adopted to filter out the negligible but nonzero coefficients of $\Pi_{\cdot \hat{e}}$. Consequently, we can calculate the estimated coordinates of targets based on $\hat{\boldsymbol{\theta}}$, and estimate the target number as $\hat{K} = \|\hat{\boldsymbol{\theta}}\|_0$.

Algorithm 1 Location Vector Estimation

- 1: **Initialization:**
 - 2: $\gamma_{\text{th}} = 10^{-3}$, $\tau_{\text{max}} = 10^3$, $\eta_{\text{th}} = -10\text{dB}$, $\gamma = \tau = 0$.
 - 3: **while** ($\gamma \geq \gamma_{\text{th}}$ or $\tau \leq \tau_{\text{max}}$) **do**
 - 4: Calculate Σ and $\mathbf{\Pi}$ by using (15)–(16).
 - 5: Update $\boldsymbol{\alpha}$ and σ^2 by using (18)–(19).
 - 6: $\gamma \leftarrow \|\mathbf{Y} - \mathbf{\Phi} \mathbf{\Pi}\|$, $\tau \leftarrow \tau + 1$.
 - 7: **end while**
 - 8: Choose \hat{e} that minimizes $\|\mathbf{y}^e - \mathbf{\Phi} \Pi_{\cdot e}\|$.
 - 9: If $20 \lg(\Pi_{n \hat{e}} / \max_i |\Pi_{i \hat{e}}|) < \eta_{\text{th}}$, set $\Pi_{n \hat{e}} = 0$ for all n .
 - 10: Let the estimated location vector $\hat{\boldsymbol{\theta}} = \Pi_{\cdot \hat{e}}$.
-

4 Numerical Results

4.1 Simulation Setup

In this section, we conduct numerical simulations to demonstrate the superior performance of MDMI. For a typical scenario of CS-based multi-target DFL, the monitoring area \mathcal{A} is set as a $14\text{m} \times 14\text{m}$ square region. \mathcal{A} is divided into $N = 784$ equal-sized grids, and the side length of each grid is 0.5m . To locate the targets, a wireless network with $M = 28$ wireless links is deployed in \mathcal{A} . The signal-to-noise ratio (SNR) is defined as $\text{SNR}(\text{dB}) \triangleq 10 \lg(\|\Phi\theta\|_2^2/M\sigma^2)$.

To evaluate the localization and counting performance, we define the following two metrics: (1) Average localization error (*AvgErr*), which denotes the average Euclidean distance between the true and estimated target locations; (2) Correct counting rate (*CoCoun*), which represents the probability of correctly estimating the target number (i.e., $\hat{K} = K$). In our simulations, we compare the localization performance of MDMI with the CS-based multi-target DFL approaches that adopt the following sparse recovery algorithms: orthogonal matching pursuit (OMP) [10], basis pursuit (BP) [8], greedy matching pursuit algorithm (GMP) [9], Bayesian compressive sensing (BCS) [14], and variational EM algorithm [11].

4.2 Impact of the Number of Iterations

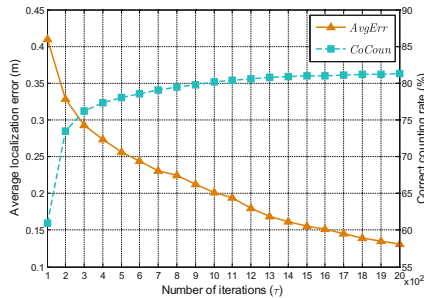


Fig. 2. The performance of MDMI when τ varies from 10^2 to 2×10^3 .

In the first simulation, we investigate the impact of the number of iterations on the performance of MDMI. In Sect. 3, an iterative two-step procedure is adopted to estimate the posterior of \mathbf{w}^e and the parameters α and σ^2 . Intuitively, the estimation accuracy is closely related to the iteration number τ . To verify this, we test the performance of MDMI when τ varies from 10^2 to 2×10^3 . As can be seen from Fig. 2, *AvgErr* decreases rapidly as the increasing of τ . At the same time, *CoCoun* is increased. The simulation results confirm our analysis. Although we can achieve a better performance with a larger τ , it may result in heavy computational load. For this reason, we set $\tau_{\max} = 10^3$ as a tradeoff between accuracy and complexity.

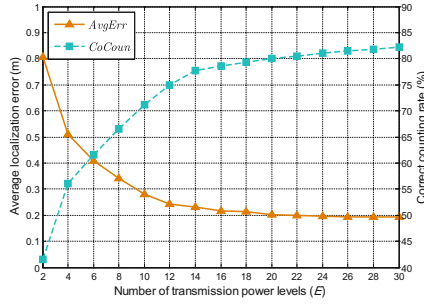


Fig. 3. The performance of MDMI when E varies from 2 to 30.

4.3 Impact of the Number of Transmission Power Levels

In the second simulation, we test the effect of the number of transmission power levels on the target localization and counting performance. The key novelty of the proposed MDMI is the utilization of the RSS measurements that collected from multiple transmission power levels. If we increase the number of transmission power level E , the power diversity of RSS measurements will be improved, and more useful information will be provided. To validate the effectiveness of MDMI, we conduct a quantitative analysis to investigate how the number of transmission power levels affects the localization and counting performance. Figure 3 shows $AvgErr$ and $CoCoun$ under different values of E . The simulation results confirm the effectiveness of MDMI. However, it is noteworthy that $AvgErr$ decreases very slowly when E exceeds 20. When $E > 20$, the negative effect of increasing the transmission power level will almost offset the positive effect contributed by power diversity. In view of this, we choose $E = 20$ in the following simulations.

4.4 Localization Error vs. Number of Targets

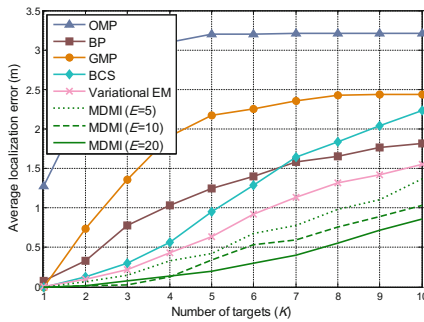


Fig. 4. Impact of the number of targets on average localization error.

In the third simulation, we turn our attention to the impact of the number of targets on localization accuracy. Figure 4 shows the performances of multiple DFL approaches under different numbers of targets. When K increases from 1 to 10, the $AvgErr$ for all approaches increase dramatically. It should be pointed out that, with the increase in K , the joint sparsity level of $\{\mathbf{w}^e\}_{e=1}^E$ will decrease accordingly. In this case, the reconstruction accuracy of the location vector will be degraded according to the principle of CS. Furthermore, owing to the aggregating of multidimensional measurement information, MDMI can achieve the lowest $AvgErr$ among all approaches.

4.5 Localization Error vs. SNR

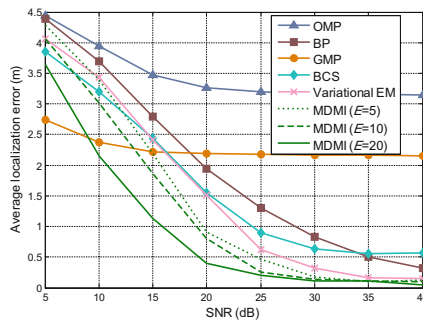


Fig. 5. Impact of the signal-to-noise ratio on average localization error.

In the last simulation, the localization performances of DFL approaches under different SNR is demonstrated. Figure 5 shows the results of the simulation. As SNR increases from 5 to 40 dB, the $AvgErr$ of all DFL methods experience a greatly drop. We observe that the MDMI($E = 20$) outperforms other DFL methods in most cases ($SNR > 9$ dB). In addition, when $SNR < 30$ dB, the difference in $AvgErr$ among MDMI($E = 5$), MDMI($E = 10$) and MDMI($E = 20$) is relatively high. This implies that we can mitigate the influence of measurement noise by increasing the power diversity of RSS measurements.

5 Conclusion

In this paper, a novel CS-based multi-target DFL method (MDMI) is developed to reduce the number of wireless links that required for multi-target DFL. Unlike existing CS-based DFL methods for multiple targets which collect measurements from just one transmission power level, MDMI proposes to exploit multidimensional wireless link information from multiple transmission power levels. It models the CS-based multi-target DFL problem as a joint sparse recovery problem,

and adopts the multiple sparse Bayesian learning (M-SBL) algorithm to reconstruct the sparse vectors of different transmission power levels. To validate the merits of MDMI, we perform an extensive simulation study compared with the state-of-the-art CS-based multi-target DFL approaches. Simulation results confirm the effectiveness of the proposed method.

Acknowledgment. This work was supported in part by the National Natural Science Foundation of China under grant 61871400, and 61571463; the Natural Science Foundation of Jiangsu Province under grant BK20171401.

References

1. Khalajmehrabadi, A., Gatsis, N., Akopian, D.: Modern WLAN fingerprinting indoor positioning methods and deployment challenges. *IEEE Commun. Surv. Tuts.* **19**(3), 1974–2002 (2017). <https://doi.org/10.1109/COMST.2017.2671454>
2. Wang, J., Gao, Q., Pan, M., Fang, Y.: Device-free wireless sensing: challenges, opportunities, and applications. *IEEE Netw.* **32**(2), 132–137 (2018). <https://doi.org/10.1109/mnet.2017.1700133>
3. Lei, Q., Zhang, H., Sun, H., Tang, L.: Fingerprint-based device-free localization in changing environments using enhanced channel selection and logistic regression. *IEEE Access* **66**, 2569–2577 (2018). <https://doi.org/10.1109/ACCESS.2017.2784387>
4. Zhou, Z., Wu, C., Yang, Z., Liu, Y.: Sensorless sensing with WiFi. *Tsinghua Sci. Technol.* **20**(1), 1–6 (2015). <https://doi.org/10.1109/tst.2015.7040509>
5. Zhang, D., et al.: Fine-grained localization for multiple transceiver-free objects by using RF-based technologies. *IEEE Trans. Parallel Distrib. Syst.* **25**(6), 1464–1475 (2014). <https://doi.org/10.1109/tpds.2013.243>
6. Zhang, D., Liu, Y., Guo, X., Ni, L.: RASS: a real-time, accurate, and scalable system for tracking transceiver-free objects. *IEEE Trans. Parallel Distrib. Syst.* **24**(5), 996–1008 (2013). <https://doi.org/10.1109/tpds.2012.134>
7. Wang, Q., Yigitler, H., Jantti, R., Huang, X.: Localizing multiple objects using radio tomographic imaging technology. *IEEE Trans. Veh. Technol.* **65**(5), 3641–3656 (2016). <https://doi.org/10.1109/tvt.2015.2432038>
8. Candes, E., Wakin, M.: An introduction to compressive sampling. *IEEE Signal Process. Mag.* **25**(2), 21–30 (2008). <https://doi.org/10.1109/msp.2007.914731>
9. Wang, J., Fang, D., Chen, X., Yang, Z., Xing, T., Cai, L.: LCS: compressive sensing based device-free localization for multiple targets in sensor networks. In: *IEEE INFOCOM 2013*, Turin, Italy, pp. 14–19 (2013). <https://doi.org/10.1109/infcom.2013.6566752>
10. Wang, J., et al.: E-HIPA: an energy-efficient framework for high-precision multi-target-adaptive device-free localization. *IEEE Trans. Mob. Comput.* **16**(3), 716–729 (2017). <https://doi.org/10.1109/tmc.2016.2567396>
11. Yu, D., Guo, Y., Li, N., Fang, D.: Dictionary refinement for compressive sensing based device-free localization via the variational EM algorithm. *IEEE Access* **4**, 9743–9757 (2016). <https://doi.org/10.1109/access.2017.2649540>
12. Wipf, D., Rao, B.: An empirical Bayesian strategy for solving the simultaneous sparse approximation problem. *IEEE Trans. Signal Process.* **55**(7), 3704–3716 (2007). <https://doi.org/10.1109/TSP.2007.894265>

13. Wang, J., Gao, Q., Pan, M., Zhang, X., Yu, Y., Wang, H.: Towards accurate device-free wireless localization with a saddle surface model. *IEEE Trans. Veh. Technol.* **65**(8), 6665–6677 (2016). <https://doi.org/10.1109/tvt.2015.2476495>
14. Ji, S., Xue, Y., Carin, L.: Bayesian compressive sensing. *IEEE Trans. Signal Process.* **56**(6), 2346–2356 (2008). <https://doi.org/10.1109/TSP.2007.914345>